A multiplexing system for quantifying oxygen fractionation factors in closed chambers

Clémence Paul[1], Clément Piel[2], Joana Sauze[2], Olivier Jossoud[1,] Arnaud Dapoigny[1], Daniele Romanini[4], Frédéric Prié[1], Sébastien Devidal[2], Roxanne Jacob[1], Alexandru Milcu[2,3], Amaëlle Landais[1]

[1] Laboratoire des Sciences du Climat et de l'Environnement, LSCE - IPSL, CEA-CNRS-UVSQ, Université Paris-Saclay, 91191 Gif-sur-Yvette, France

[2]Ecotron Européen de Montpellier (UAR 3248), Univ Montpellier, Centre National de la Recherche Scientifique (CNRS), Campus Baillarguet, Montferrier-sur-Lez, France

[3] CEFE, Univ Montpellier, CNRS, EPHE, IRD, Montpellier, France

[4]Laboratoire Interdisciplinaire de Physique, Univ Grenoble Alpes, CNRS/UGA, Saint-Martin-d'Hères, France

Correspondence: Clémence Paul (clemence.paul@lsce.ipsl.fr)

Abstract

The study of isotopic ratios of atmospheric oxygen in fossilized air trapped in ice core bubbles provides information on variations in the hydrological cycle at low latitudes and productivity in the past. However, to refine these interpretations, it is necessary to better quantify fractionation of oxygen in the biological processes such as photosynthesis and respiration. We set up a system of closed biological chambers in which we studied the evolution of elemental and isotopic composition of O_2 due to biological processes. To easily replicate experiments, we developed a multiplexing system which we describe here. We compared measurements of elemental and isotopic composition of O_2 using two different measurement techniques: optical spectrometry (Optical-Feedback Cavity- Enhanced Absorption Spectroscopy, i.e. OF-CEAS technique), which enables higher temporal resolution and continuous data collection and isotopic ratio mass spectrometry (IRMS) with a flanged air recovery system, thus validating the data analysis conducted through the OF-CEAS technique. As a first application, we investigated isotopic discrimination during respiration and photosynthesis. We

conducted a 5-day experiment using maize (*Zea mays* L.) as model species. The ^{18}O discrimination value for maize during dark plant respiration was determined as - 17.8 ± 0.9 ‰ by IRMS and - 16.1 ± 1.1 ‰ by optical spectrometer. We also found a value attributed to the isotopic discrimination of terrestrial photosynthesis equal to + 3.2 ± 2.6 ‰ by IRMS and + 6.7 ± 3.8 ‰ by optical spectrometer. These findings were consistent with a previous study by Paul et al. (2023).

1. Introduction

Oxygen, the most abundant chemical element on Earth, is present in all the geological layers, both internally and externally. In the surface layers of the Earth (atmosphere, biosphere, ocean), it is produced from water through the well-known biological process of photosynthesis. Consumption of O_2 is mainly due to respiration. The photosynthesis and respiration fluxes are responsible for the seasonal variations of dioxygen concentration in the atmosphere (Keeling and Shertz, 1992) and play a role in the longer-term evolution of O_2 (Stolper et al., 2016). Oxygen consists of three stable isotopes: ^{16}O, ^{17}O and ^{18}O. By measuring the ratios of these isotopes, we can document the physicochemical and biological processes involved in the oxygen cycle. We use the $\delta^{18}O$ notation to express the isotopic signal of oxygen compared to a reference isotopic ratio (Eq. 1):

$$\delta^{18}O_{calibrated} = \left[\frac{\left(\frac{^{18}O}{^{16}O}\right)_{sample}}{\left(\frac{^{18}O}{^{16}O}\right)_{standard}} - 1 \right] \times 1000 \quad (1)$$

Oxygen isotopes do not have the same thermodynamic properties. Thus, during phase changes, fractionation occurs which is measured by the fractionation factor α (Eq. 2):

$$^{18}\alpha = \frac{^{18}R_{product}}{^{18}R_{substrate}} \quad (2)$$

where ^{18}R is the ratio of the concentration $^{18}R = \frac{n(^{18}O)}{n(^{16}O)}$ and n the number of moles of O_2 containing ^{18}O or ^{16}O.

The isotopic discrimination is related to the isotopic fractionation factor through:

$$^{18}\varepsilon = {}^{18}\alpha - 1 \quad (3)$$

The isotopic composition of dioxygen in the atmosphere, $\delta^{18}O$ of O_2 in air, is often noted $\delta^{18}O_{atm}$. This signal, measured in the air bubbles in ice cores, can be used for ice core dating, related to the past variations of the hydrological cycle of water in the low latitudes and the relative proportion of oceanic

vs terrestrial productivity. First, using the analyses of isotopic composition of dioxygen in the air trapped in ice cores, Bender et al. (1994) demonstrated that $\delta^{18}O_{atm}$ varies synchronously with precession, a discovery that has been instrumental in using this proxy for dating ice cores (Petit et al., 1999; Dreyfus et al., 2007). This influence of precession on $\delta^{18}O_{atm}$ is possibly due to changes in the low-latitude hydrological cycle driven by precession (Bender et al., 1994; Severinghaus et al., 2009; Landais et al., 2010; Seltzer et al., 2017). Such variations in low-latitude hydrological cycle influence the $\delta^{18}O$ of meteoric water which is then transmitted to the $\delta^{18}O_{atm}$ through terrestrial photosynthesis. Supporting this, over the past 650,000 years, $\delta^{18}O_{atm}$ has shown a strong correlation with $\delta^{18}O_{calcite}$ variations in East Asian speleothems (Wang et al., 2008; Cheng et al., 2016), which are largely controlled by shifts in the low-latitude water cycle, particularly monsoonal activity.

The interpretation of $\delta^{18}O_{atm}$ as an indicator for reconstructing oceanic and terrestrial productivity relies on the definition of the Dole effect (DE) calculated as the difference between $\delta^{18}O_{atm}$ and $\delta^{18}O_{sw}$ (sw referring to sea water). The present Dole effect has a value which is estimated to 24 ‰ (Bender et al., 1994; Hoffmann et al., 2004; Luz and Barkan, 2011).

Bender et al. (1994), Malaizé et al. (1999) and Hoffmann et al. (2004) proposed that changes in the Dole effect are driven by the relative contribution of terrestrial and oceanic productivity. This conclusion arises from the fact that the terrestrial Dole effect defined as the enrichment of atmospheric O_2 $\delta^{18}O$ relative to $\delta^{18}O_{sw}$ due to terrestrial biosphere fluxes is estimated to be several permil higher than the oceanic Dole effect, which results from oceanic biosphere fluxes. This conclusion is based on of the available determinations of O_2 fractionation coefficients associated with biological processes, including terrestrial and oceanic respiration and photosynthesis (Guy et al., 1993; Angert and Luz, 2001; Hendricks et al., 2004; Helman et al., 2005)). In contrast, Luz and Barkan (2011) used updated estimates of O_2 fractionation coefficients and arrived at a different conclusion: both the terrestrial and oceanic Dole effects are approximately 24 ‰. It is thus of primary importance to determine robust values of fractionation coefficients of O_2 during biological processes.

Previous studies conducted over previous decades at the cell or organism level (Guy et al., 1993; Angert et al., 2001; Helman et al., 2005; Eisenstadt et al., 2010; Stolper et al., 2018) have already revealed variations in oxygen fractionation among different biological species and methods employed. Guy et al. (1993) conducted investigations on spinach thylakoids, cyanobacteria (*Anacystis nidulans*) and diatoms (*Phaeodactylum tricornutum*), and estimated a respiratory discrimination of oxygen by about 21 ‰. Kroopnick and Craig (1972) measured this effect on plankton incubated in natural seawater and obtained a similar value. Luz and Barkan (2002) found a respiratory fractionation of 21.6 ‰ on incubation experiments with natural plankton in Lake Kinneret. Finally, the global average oceanic

respiratory fractionation value given by Luz and Barkan (2011) is 19.7 ‰ on samples from the Celtic Sea, Southern Ocean, North Atlantic and Red Sea. For terrestrial respiration, using a compilation of values from previous experiments, Bender et al. (1994) gave a global respiratory fractionation value of 18 ‰. Angert et al. (2001) focused on soil samples and gave a soil respiratory fractionation (roots and micro-organisms) of around 12 ‰. This lower value is the result of the role of roots in limiting oxygen diffusion in the consumption site.

Guy et al. (1993) showed that photosynthesis does not fractionate oxygen between the water consumed and the dioxygen produced by the organism. However, Eisenstadt et al. (2010) found later a discrimination up to 6 ‰ for oceanic photosynthesis on a study on oceanic phytoplankton, whereas Paul et al. (2023) found a discrimination of 3.7 ± 1.3 ‰ for terrestrial photosynthesis with an experiment performed at the scale of a terrarium with *Festuca arundinacea.* Such different contributions lead to different interpretation of past variations in $\delta^{18}O_{atm}$ or Dole effect.

The variety of values found for the different studies can be attributed to the different set-up used, different environment or different species. To determine robust values of fractionation coefficients, it is necessary to proceed in a systematic way and use the same set-up for a large variety of plants and environments which is the goal of the set-up detailed in this study.

Finally, note that isotopic composition of O_2 can be used to quantify global biosphere productivity (Bender et al., 1994; Luz et al., 1999; Severinghaus et al., 2009; Brandon et al., 2020; Yang et al., 2022). Such reconstruction relies on the observation that biological productivity processes (respiration and photosynthesis) fractionate oxygen in a mass dependent manner (i.e. there is a consistent relationship between changes in $\delta^{17}O$ and $\delta^{18}O$, approximately equal to 0.5), while dioxygen originating from exchanges with the stratosphere has an isotopic composition affected by mass independent fractionation (hence a relationship between changes in $\delta^{17}O$ and $\delta^{18}O$ significantly different from 0.5 i.e. between 1 and 2). The relative proportion of biosphere productivity vs stratospheric exchange fluxes sets the value of the relationship between $\delta^{17}O$ vs $\delta^{18}O$ in the troposphere, which is often described as $\Delta^{17}O = \ln(1 + \delta^{17}O) - 0.516 \times \ln(1 + \delta^{18}O)$ (Luz et al., 1999). In parallel, the same parameter $\Delta^{17}O$ measured in the air dissolved in the ocean permits to constrain the gross biosphere productivity when combined with the concentration of O_2 measured as the ratio O_2/Ar (Luz et al., 2000).

Although our system can in theory enable determination of the triple isotopic composition of O_2 (through IRMS, Isotopic Ratio Mass Spectrometry), we will focus on $\delta^{18}O$ of O_2 in the present study. We thus concentrate on fractionation coefficients needed to interpret $\delta^{18}O_{atm}$ records only.

In this study, we present an automated setup which can be used to perform numerous systematic studies of the fractionation factor of oxygen during biological processes. Similar to the study of Paul et al. (2023), we used closed growth chambers to quantify oxygen fractionation factors associated with respiration and photosynthesis of *Festuca arundinacea*. The novelty is that we worked with up to three closed chambers simultaneously in an automated way which allows an exploration of numerous different plant species and climatic conditions. Moreover, the isotopic analyses are now performed with an optical spectrometer (Optical-Feedback Cavity-Enhanced Absorption Spectroscopy, i.e. OF-CEAS technique) in addition to IRMS. This spectrometer allows studying the concentration and the isotopic composition of O_2 in the different chambers in a continuous way.

This manuscript is organized as follows. First, we will present new developments on closed biological chambers compared to the study of Paul et al. (2023) as well as the multiplexing system integrating continuous measurements of elemental and isotopic composition of O_2. Then, we will present the results of a biological experiment where photosynthesis and respiration took place. Finally, we will provide estimate of fractionation factors through two analytical techniques: optical spectrometry and IRMS.

2. Material and Methods

2.1. Growth chamber and closed system

A set of three airtight transparent welded polycarbonate chambers (120 L volume) were adapted from the chamber described in Paul et al. (2023) and Milcu et al. (2013). The main controlled environmental parameters inside the closed chambers were temperature, light intensity, CO_2 concentration, relative humidity and differential pressure.

CO_2 mixing ratio during light period (dominated by photosynthesis) was regulated with short (30s) pulses of pure CO_2 provided at regular intervals (90s for a sequence with 3 chambers) to each chamber using a mass flow controller (F200CV, Bronkhorst, The Netherlands) and a Valco selector (EUTF-SD12MWE, VICI AG International, Switzerland). During the dark period (dominated by plant and soil respiration), the CO_2 is trapped through a 0.5-liter cylinder filled with soda lime and was connected to a NMS020B KNF micropump.

Unlike the system described in Paul et al. (2023) (Fig.1), relative humidity in each chamber was controlled using a thermoelectric cooler (100 watt, ET-161-12-08-E Adaptive). The cooled side of the

cooler was in thermal contact with an aluminum rod (1.5 cm diameter) connected to a heat exchanger acting as condenser inside the chamber. The temperature of the condenser block was monitored with a thermistor, and the condensed water was directed to the plastic tray containing the plant using an 8 mm plastic tube.

Each chamber was used as a closed gas exchange system, and placed in a separate controlled environment growth chamber, in the Microcosms experimental platform of the Montpellier European Ecotron. The temperature of the growth chamber was automatically adjusted in order to keep constant the temperature at 20°C inside the closed chamber (growth chamber usually set between 20 and 21°C during dark period and around 18°C during light period because of the greenhouse effect in the chamber). Air and soil temperature were monitored using 4 NTC probes (CTN 35, Carel). Air relative humidity and temperature were monitored with a capacitive humidity sensor and a PT100 (PFmini72, Mitchell Instruments, USA). Air CO_2 mixing ratio was monitored using a K30 probes (K30, Senseair).

To find potential leaks in each chamber, helium tests were performed before each experiment.

a)

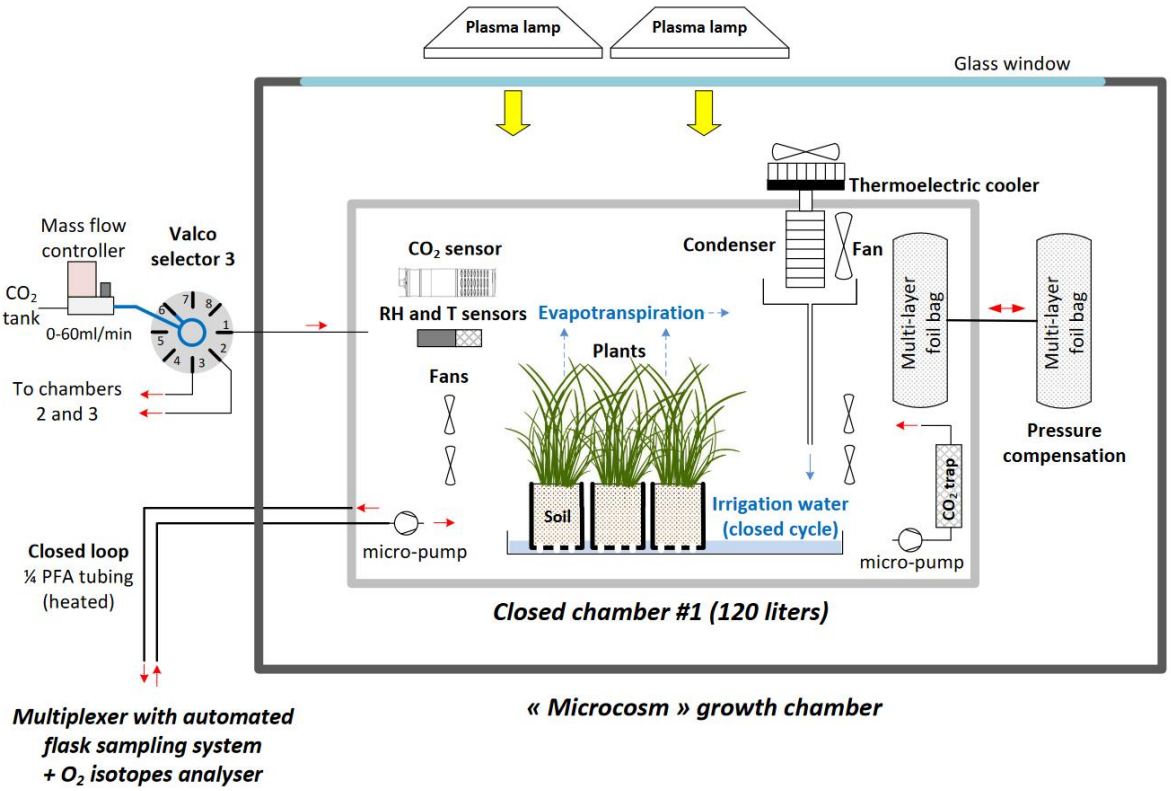
Plasma lamp
Plasma lamp
Glass window
Thermoelectric cooler
Mass flow controller
Valco selector 3
CO_2 tank
0-60ml/min
To chambers 2 and 3
CO_2 sensor
RH and T sensors
Evapotranspiration
Condenser
Fan
Multi-layer foil bag
Multi-layer foil bag
Pressure compensation
Plants
Fans
Soil
Irrigation water (closed cycle)
CO_2 trap
micro-pump
micro-pump
Closed loop ¼ PFA tubing (heated)
Closed chamber #1 (120 liters)
Multiplexer with automated flask sampling system + O_2 isotopes analyser
« Microcosm » growth chamber

b)

Fig.1. The set-up of the closed chamber system hosting a vegetation-soil atmosphere analogue of the terrestrial biosphere. (a) Schematic of the closed chamber setup used for the terrestrial biosphere model. The closed chamber was enclosed in a larger growth chamber. Main environmental parameters inside the closed chamber were actively controlled and monitored: temperature (T), light intensity, CO_2, relative humidity (RH), pressure differential (ΔP). The water cycle in the closed chamber is shown in blue. (b) Photograph of the closed chamber used in the experiment with *Zea Mays.*

2.2. Multiplexing system

With this set-up, we continuously measured the isotopic composition of O_2 using an online optical spectroscopy instrument, hereafter the isotopic analyzer. For each chamber, air circulated through two external closed loops connected by a tee. The first loop is made of 1/8-inch PFA tubing and used a Valco selector (12 positions 1/8 inch, EUTF-SD12MWE, VICI AG International, Switzerland) to enable the air to circulate from one closed chamber through the isotopic analyzer and back to the closed chamber (Fig.2). The Valco valve selected the origin of the air to be sent to the isotopic analyzer. Five different origins can be selected (but more can be added): three different closed system chambers and two reference gases ((1) dried atmospheric air (with a magnesium perchlorate trap), (2) synthetic air (Alphagaz 2, Air Liquide, France) or dry natural air with 23 % O_2 (Natural Air, Air Liquide Espana, Spain)). Air at the entrance of the isotopic analyzer was dried with a 20 cm long trap (6 mm PFA tube filled with magnesium perchlorate, renewed daily), and filtered (Millex-FH 0.45 µm/50 mm PTFE hydrophobic filter, Merck, Germany).

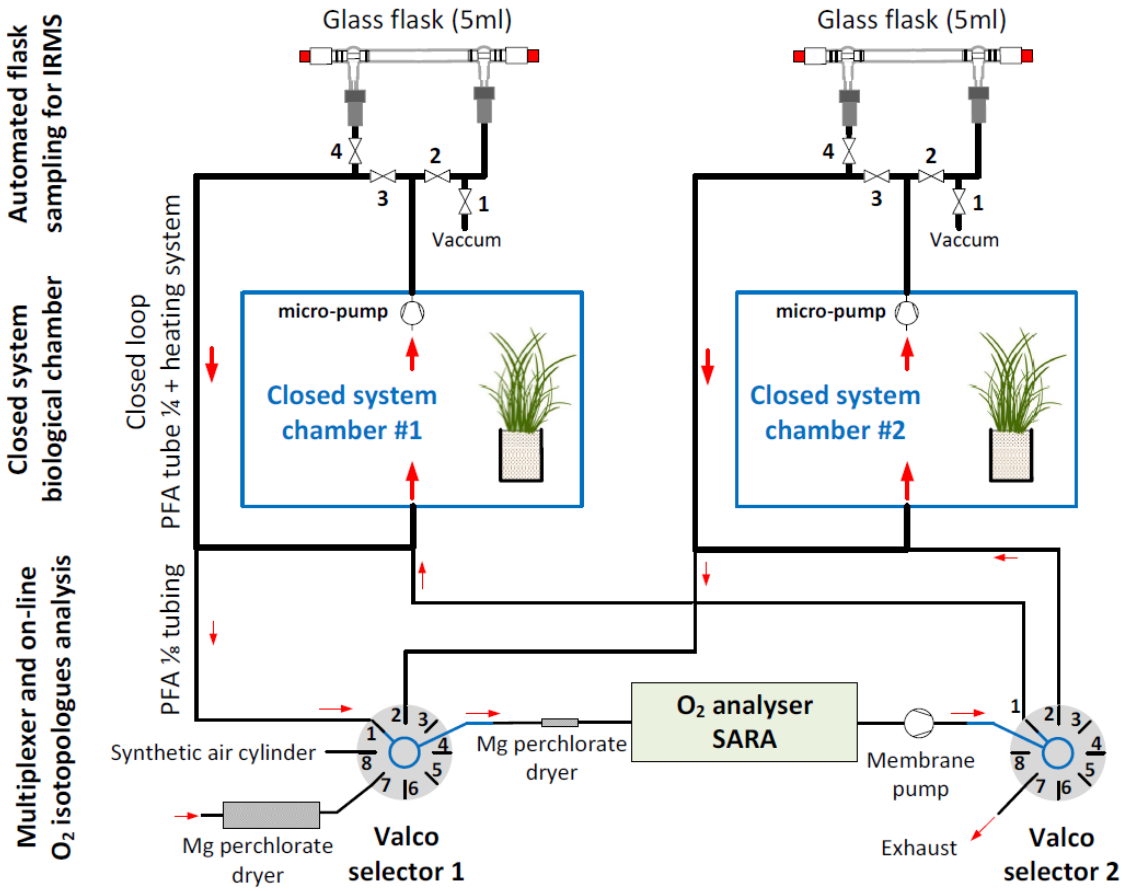

Fig.2. Diagram of the multiplexing system: the enclosed atmosphere of three biological system chambers circulates through automated flask sampling systems using loops employing ¼" PFA tubing and micro-pumps. Subsequently, air from these loops is sub-sampled using 1/8-inch PFA tubes and Valco selectors and analyzed with an isotope analyzer.

Once analyzed, the air stream entered a membrane pump (N811KN.18, KNF, Germany), and subsequently the common port of a second Valco selector (12 positions 1/8 inch, EUTF-SD12MWE, VICI AG International, Switzerland). The air was then either redirected to its chamber of origin (closed circuit) or vented outside of the chamber through an exhaust port for the calibration gases. The multiplexer composed of two Valco valves ensure three functions : (1) "calibration" : dried ambient air or synthetic air is provided to the spectrometer, and the outlet is vented to the atmosphere, (2) "purge": the remaining air still present inside the spectrometer is vented to the atmosphere, until it is fully replaced by the new stream of air (in order to avoid cross contamination of the air between chambers, or contamination of a given chamber with the calibration stream), (3) "measurement": the air sub-sampled from a given chamber is flowing through the spectrometer, and then back to the chamber. A typical sequence is described in Table 1.

Table 1. Typical measurement sequence with the optical spectrometer. Note that a small amount (around 5 mL) of air sampled from the chamber is wasted (Valco 2 exhausts to atmosphere) during the purging phase.

Phase	Duration (s)	Valco 1 (Port selected)	Valco 2 (Port selected)	Targeted chamber
Calibration	300	7	7	-
Purge	20	1	7	1
Measurement	280	1	1	1
Calibration	300	7	7	-
Purge	20	2	7	2
Measurement	280	2	2	2
Calibration	300	7	7	-
Purge	20	3	7	3
Measurement	280	3	3	3

The second loop, used in parallel to the first one described above, is dedicated to the sampling of air for further analysis by IRMS, as already done in Paul et al. (2023) (Fig.2). Air sampled from each chamber was circulating continuously into a closed loop (PFA tubing, 1/4-inch, total length between 5 and 10m depending on the chamber location relative to the measurement system) using a micropump with a flow rate of approximatively 1 L/min (NMS020B, KNF, Germany), through an automated flask sampling system. All tubes were heated using self-regulating heating cable (15 W m^{-1}, Technitrace, France), and the sampling system was located in a temperature regulated enclosure (25 to 30°C). The sampling system was made of two three-way pneumatic valves for each chamber (M8.1 VBV, Rotarex) connected to a glass flask (5mL, as described in Paul et al. (2023)) with two Ultra-Torr fittings (SS-4-UT-9, Swagelok, USA) and ensured three functions as described in Table 1: (2) “Purge”: the flask is isolated from the closed loop and connected to a vacuum pump (1 to 5 mbar), (2) “Sampling”: the air from the loop is flowing through the sampling flask and back to the loop, (3) “Hold”: the flask is isolated from the closed loop in order to be manually closed and collected. During a typical sequence, each flask was evacuated (“purge”) for 10 minutes, then the “sampling” was activated for at least 30 minutes, and “hold” was triggered at a time selected by the user using a computer-controlled system (Table 2).

Table 2. Sampling sequence with the flask sampling system.

State	Valves				Air flow	Duration (min)
	1	2	3	4		
Purge	Open	Closed	Open	Closed	Flask bypassed	10
Sampling	Closed	Open	Closed	Open	Through flask	30
Hold	Closed	Closed	Open	Closed	Flask bypassed	to be adjusted

2.2.2. Description of control commands

The control software was developed using open-source Python libraries (PyQt5 for the GUI) and homemade drivers to interact with the various elements (valves, sensors, regulators, etc.) through serial connections. It included a user interface displaying the state of relevant components and the value of the different sensors. The software had three main functions:

- controlling the chamber's CO_2 injection rate: the desired CO_2 rate target can be set and the automatic regulation can be turned on or off using the GUI (Graphical User Interface). The CO_2 trap state and the CO_2 injection flow rate were also displayed. Real-time plots showed the CO_2 in ppm of each chamber, for quick and easy visual control.

- controlling the flow path of the optical spectrometry analyzer, by sending commands to the upstream and downstream valves. A sequencer can be used to define how long and in which order the chambers or calibration gases should be measured by the optical spectrometer.

- controlling the flask sampling. This part controls the pneumatic valves which create the flow path for purging, filling or holding the content of the flask. The duration of the purge and the absolute timestamp of the sampling can be set individually for each chamber, for automatic sampling, while manual operation is still possible.

Furthermore, the control software retrieved concentration data from the optical spectrometer via an Ethernet connection and merged it with the flow path data into an unified, time-consistent file for convenient future analysis.

2.2.3. Mass spectrometry and optical spectrometry analyses

2.2.3.1. Mass spectrometry analyses technique

In order to be able to compare the evolutions of $\delta^{18}O$ of O_2 and $\delta O_2/N_2$ measured by the mass spectrometer and the optical spectrometer during light and dark periods, we collected the air in the chamber via the flask sampling system during one dark period (night 1) and one light period (day 2). We collected 6 flasks for the dark period and 5 flasks for the light period.

The air sampled by the flask system of the second loop was transported to LSCE. The air collected was purified by a semi-automatic separation line (Capron et al., 2010) and analyzed by a Delta V plus dual inlet mass spectrometer (Thermo Electron Corporation). One run consists of 2 series of 16 measurements for each sample and measures the isotopic composition of the air: $\delta^{18}O$ of O_2 and $\delta O_2/N_2$ (Extier et al., 2018).

2.2.3.2. Optical spectrometry analyses (OF-CEAS technique)

The description of the OF-CEAS laser optical spectrometer is detailed in Piel et al. (preprint). The spectrometer measured simultaneously $\delta^{18}O$ of O_2 and O_2 mixing ratio. In our case, because of an experimental problem during the experiment, the instrument was working with a slightly deteriorated precision. Liquid water entered the instrument due to condensation in the piping connected to the instrument.

a)

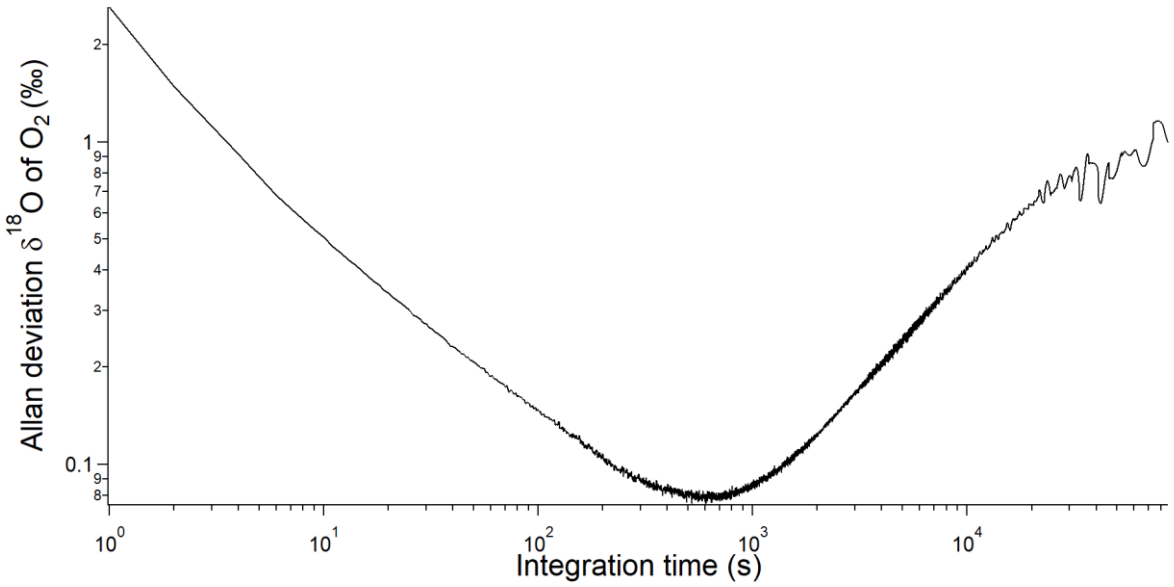

b)

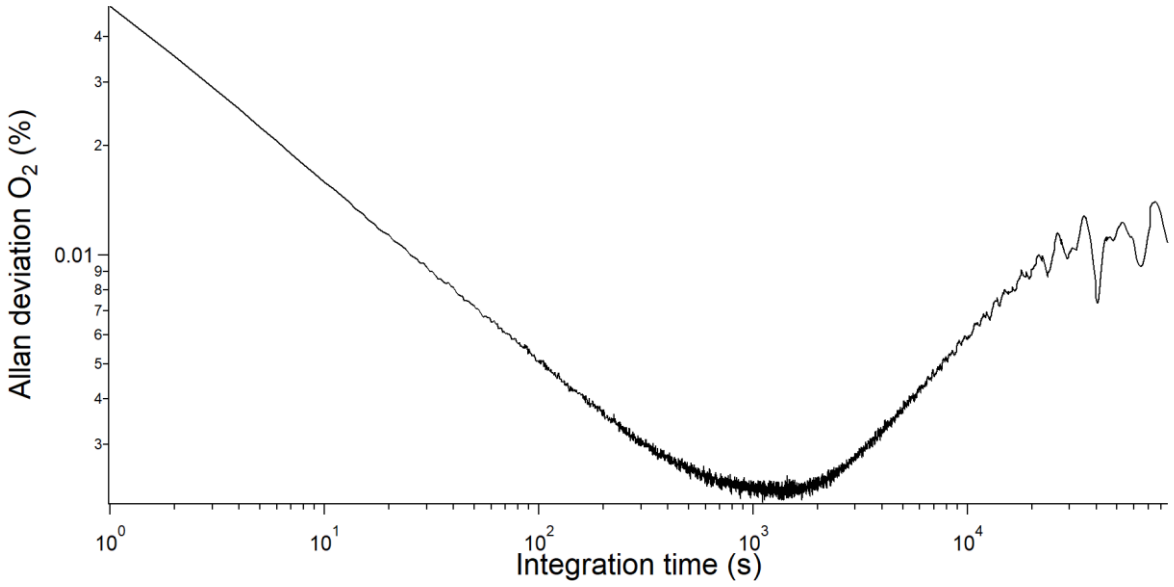

Fig. 3 Allan deviation for (a) $\delta^{18}O$ of O_2 and (b) O_2 concentration from optical spectrometry during our studies (i.e. deteriorated mode).

In order to estimate the instrument overall precision versus raw measurement integration time, we used Allan deviation which is the square root of Allan variance (Werle, 2011). The minimum of the curve can be interpreted as the best precision the instrument can achieve and the optimum integration time. In our case (Figure 3), the best precision was 0.08 ‰ and 22 ppm for $\delta^{18}O$ and O_2 mixing ratio respectively, with an optimum integration time of 10 minutes. Furthermore, the $\delta^{18}O$ of O_2 level

remains consistently below 0.1 ‰ for a duration of 20 minutes. Based on this trend, we can infer that calibrating the instrument every 20 minutes would prevent any drift-related issues.

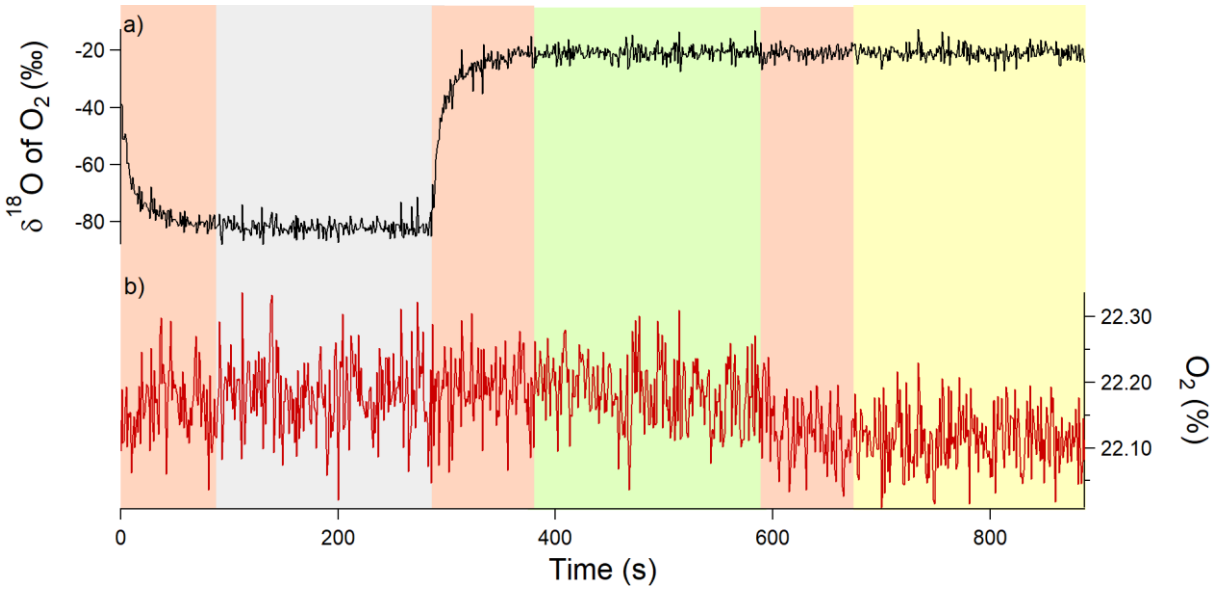

Fig.4 Example of an 18-minute measurement sequence for a closed chamber with two calibrations. Grey rectangle corresponds to calibration 1, i.e. synthetic air (with a $\delta^{18}O$ of O_2 value of - 60 ‰ measured by IRMS and with a O_2 concentration of 20.9 %), measured for 6 min. Green rectangle corresponds to calibration 2, i.e. atmospheric air (with $\delta^{18}O$ of O_2 value equal to 0 ‰ and O_2 concentration 21 %), measured for 6 min. Yellow rectangle corresponds to the air measurement of the closed chamber measured for 6 min. All the pink rectangles represent the memory effect of the analyzer, those measurement points were removed from the processed and analyzed data (i.e. first 2 minutes removed). (a) $\delta^{18}O$ of O_2 in black and (b) O_2 concentration in red.

For our sequence of measurements, we choose two calibration gases: the atmospheric air which is the reference gas and a synthetic gas which had an isotopic signature of - 60 ‰ for the $\delta^{18}O$ of O_2 and a concentration of O_2 of 23%. The sequence of measurements experiments was then: 6 min of measurement of synthetic air - 6 min of measurement of atmospheric air - 6 min of measurement of air in the chamber. This sequence was then applied to each of the 3 chambers and a full sequence lasted 18 min (Fig.4).

We had a clear memory effect when switching from one gas to another (Fig. 4). As a consequence, we removed the data of the first 2 minutes before averaging the measurements over the last 4 minutes (the instrument provided measurements at a frequency of 3 Hz) to get one averaged value. Finally, there was a dependence of $\delta^{18}O$ of O_2 on the concentration of O_2 for the spectrometry analyzer and

for this study, the correction for the influence of O_2 concentration on $\delta^{18}O$ of O_2 is given by: $\delta^{18}O_{corr}=\delta^{18}O_{measured} - (0.3736 \times [O_2] +0.0165)$ (details in Piel et al. (preprint)).

2.2.5. Experimental run

We present here the results of one experiment performed on growing maize (*Zea mays* L.) on a typical compost soil (*Terreau universel*, Botanic, France. Composition: black and blond peat, wood fibre, green compost and vermicompost manure, organic and organo-mineral fertilizers and micronutrient fertilizers) in three closed chambers in parallel. The experiment lasted 5 days, with alternating dark and light periods as follows: day 1 (6 h light) / night 1 (37 h dark) / day 2 (6 h light) / night 2 (56 h dark) / day 3 (10 h light). The dark periods were imposed to be longer than the light periods because the production rate of oxygen during photosynthesis was much stronger than the consumption rate of oxygen by respiration. Maize was chosen as the preferred option, as it is a C4 model plant and enables photosynthetic fluxes to be clearly differentiated from respiratory fluxes (no photorespiration for C4 plants), so that biological fractionation factors can be calculated easily.

2.2.4. Quantification of fractionation factors associated with respiration and photosynthesis process

In order to calculate the fractionation factors associated with dark respiration and photosynthesis of soil and maize, we used the equations 4 and 5 (for details, refer to Paul et al. (2023)).

The isotopic discrimination for dark respiration, $^{18}\varepsilon_{dark\_respi}$, is given by:

$$^{18}\varepsilon_{dark\_respi} = {}^{18}\alpha_{dark\_respi} - 1 = \frac{ln\left(\frac{\delta^{18}O_t + 1}{\delta^{18}O_{t0} + 1}\right)}{\ln\left(\frac{n(O_2)_t}{n(O_2)_{t0}}\right)} \quad (4)$$

Where $^{18}\alpha_{dark\_respi}$ is the dark respiration fractionation factor, t0 is the starting time of each dark period and t is the time of the experiment.

$\frac{n(O_2)_t}{n(O_2)_{t0}}$ is linked to $\delta\left(\frac{O_2}{N_2}\right)$ as:

$$\frac{n(O_2)_t}{n(O_2)_{t0}} = \frac{\frac{\delta\left(\frac{O_2}{N_2}\right)_t}{1000}+1}{\frac{\delta\left(\frac{O_2}{N_2}\right)_{t0}}{1000}+1} \quad (5)$$

Photosynthesis fractionation factor, $^{18}\alpha_{photosynthesis}$ is calculated as: $^{18}\varepsilon_{photosynthesis} = {}^{18}\alpha_{photosynthesis} - 1$

$$= \frac{n(O_2)_t \,/\, n(O_2)_{t0} \times a^{18}R + {}^{18}R_t \times \left(F_{photosynthesis} - F_{dark\_respi} + {}^{18}\alpha_{dark\_respi} \times F_{dark\_respi}\right)}{{}^{18}R_{lw} \times F_{photosynthesis}} \quad (6)$$

Where $a^{18}R = \frac{d^{18}R}{dt}$ during the light period, $F_{photosynthesis}$ and F_{dark_respi} are, respectively, photosynthesis and dark respiration fluxes of oxygen and *lw* stands for leaf water.

Note that because maize is a C4 plant, we consider that photorespiration and Mehler reaction were not involved in the O_2 consumption by the plant.

3. Results

3.1. Comparison between mass-spectrometry and optical-spectrometry analysis

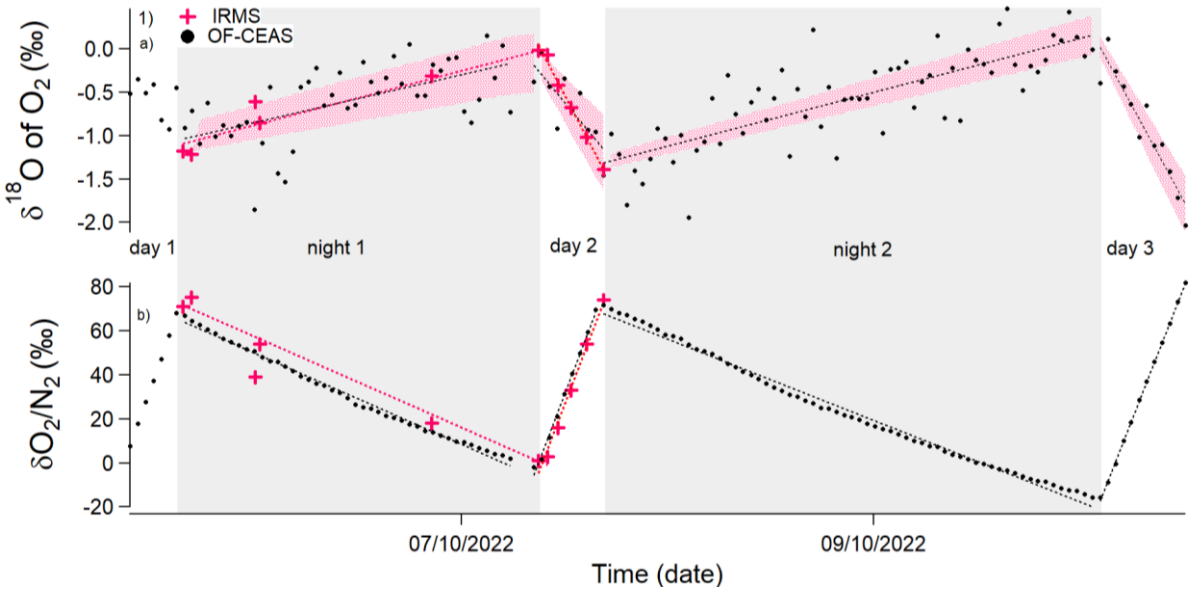

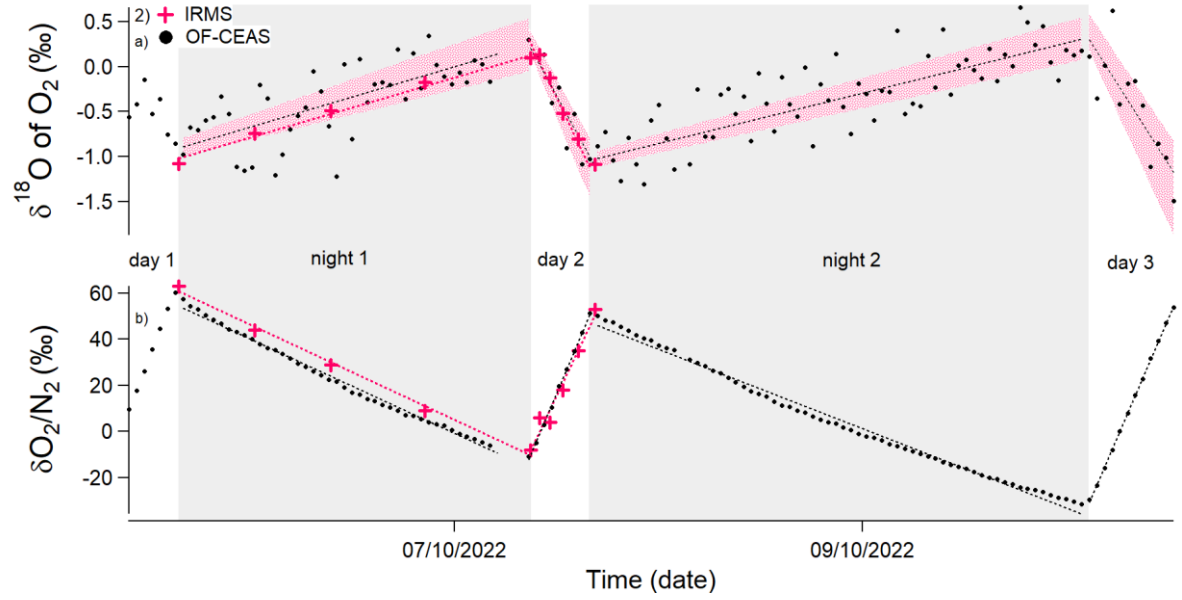

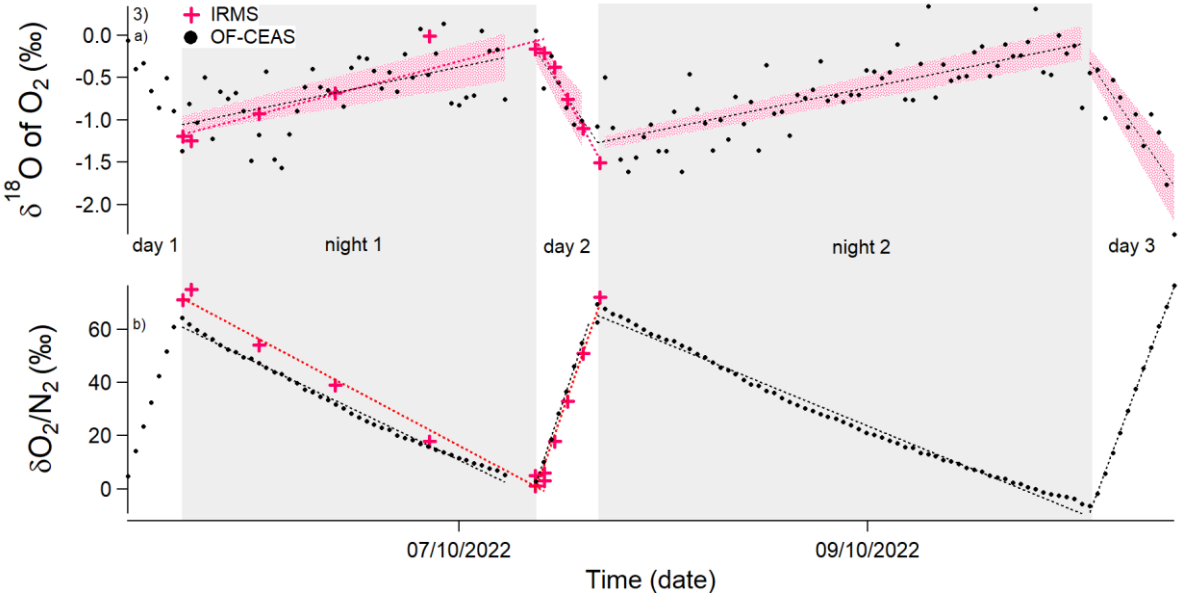

Fig.5 Evolution of the different isotopic ratios of the soil and maize experiment due to dark respiration and photosynthesis (starting 05/10/22 and ending 10/10/22) in closed chambers over 5 days. Grey rectangles correspond to dark periods and white rectangles to light periods. (1) corresponds to chamber 1, (2) chamber 2, (3) chamber 3. (a) $\delta^{18}O$ of O_2 variations. (b) $\delta O_2/N_2$ variations. Black points: optical spectrometer's data (OF-CEAS). Red stars: data obtained by IRMS. Red dashed line: linear regression of optical spectrometer data for one period (dark or light). Black dashed line: linear regression of IRMS data for one period (dark or light). Pink envelopes represent uncertainty envelops associated with linear regression slopes and intercept of optical spectrometer data for $\delta^{18}O$ of O_2. Note that the first period of light is not considered because the system is not stable at that stage.

Figure 5 presents the evolution of the elemental concentration and isotopic composition of dioxygen in the biological chambers during the experiment described in the previous section. Because of calibration, averaging and switch from one chamber to another every 18 minutes, the optical spectrometry analyzer provides only one $\delta^{18}O$ of O_2 and O_2 concentration value every 54 minutes in each chamber.

During dark periods, when there was only soil and plant respiration, $\delta^{18}O$ of O_2 increased by 1 ‰ and $\delta O_2/N_2$ decreased by 50-60 ‰ (Fig. 5). During the light period, when both photosynthesis of plant and respiration in the plant and soil occurred, the $\delta^{18}O$ of O_2 decreased by 1 ‰ and $\delta O_2/N_2$ increased by around 50 ‰ at a rate twice as fast as the decrease of respiration rate observed during nigh periods.

In Figure 5, the optical spectrometer-derived $\delta^{18}O$ of O_2 data displayed a higher degree of scattering compared to the data obtained through the use of IRMS. Nonetheless, the regression slopes computed for each period (dark and light period) demonstrate a general comparability, regardless of whether they are derived from the IRMS or optical spectrometer data (see Table 3). This finding holds significant importance as the fractionation factors were determined based on the values of these regression slopes.

Table 3. Average and standard deviation of the isotopic discriminations of maize and the number of data for all the experiment (with data of the three chambers) on which they were calculated

Isotopic discriminations of maize	Average (‰) and standard deviation		Number of data	
	IRMS	OF-CEAS	IRMS	OF-CEAS
$^{18}\varepsilon_{dark\_respi}$	- 17.8 ± 0.9	- 15.9 ± 1.4	21	57
$^{18}\varepsilon_{photosynthesis}$	3.2 ± 2.6	6.2 ± 3.3	18	249

From the results displayed on Figure 5, it was possible to calculate the isotopic discrimination found for dark respiration as $^{18}\varepsilon_{dark\_respi}$ - 17.8 ± 0.9 ‰ and- 15.9 ± 1.4 ‰ for IRMS and optical spectrometer respectively (Table 4). For photosynthesis, the isotopic discrimination found for $^{18}\varepsilon_{photosynthesis}$, is + 3.2 ± 2.6 ‰ and + 6.2 ± 3.3 ‰, for IRMS and optical spectrometer respectively.

4- Discussion

The value of isotopic discrimination, $^{18}\varepsilon_{dark\_respi}$, associated with maize growing on soil agreed with the literature. Guy et al. (1989) found a value equal to - 17 and - 19 ‰ for $^{18}\varepsilon_{dark\_respi}$ for Phaeodactylum tricornutum and terrestrial plants. Helman et al. (2005) found a value of $^{18}\varepsilon_{dark\_respi}$ equal to -17.1 ‰ for bacteria from the Lake Kinneret and a value of - 19.4 ‰ for *Synechocystis*. Paul et al. (2023), found, for *Festuca arundinacea* a value equal to - 19.1 ± 2.4 ‰.

Our value of $^{18}\varepsilon_{photosynthesis}$ for maize is also close to the value determined by Paul et al. (2023): + 3.7 ± 1.3 ‰ for *Festuca arundinacea* species. In both cases we observe a positive value which contradicts the value classically used of 0 ‰ from Guy et al. (1993). Our value hence confirms the existence of an apparent isotopic discrimination for terrestrial photosynthesis. This leads to an increase of the $\delta^{18}O$ of O_2 value associated with terrestrial biosphere compared to the latest study of Luz and Barkan (2011). As a consequence, it is still an open question to know of $\delta^{18}O_{atm}$ and Dole effectvariations should be interpreted solely as a change in the low latitude atmospheric water cycle or if the relative change in the marine vs terrestrial biological productivity also plays a role. Future studies should hence use a set-up similar to ours to systematically study the O_2 fractionation coefficients associated with biological processes.

5- Conclusions and perspectives

We have developed and presented a new automated multiplexing system that facilitates the study of gas exchange between plants and the atmosphere. This system offers several key advantages. First, it allows continuous measurements of the isotopic and elemental composition of dioxygen in the biological chamber, removing the need for manual sampling. Second, it provides near-real-time monitoring of $\delta^{18}O$ of O_2 and O_2 concentration during experiments, enabling adjustments to environmental conditions, such as dark and light cycles, in real time. Finally, it supports the convenient replication of experiments, enabling systematic studies across a wide range of environmental conditions, plant species, and soil types.

In the application of this system to maize, the fractionation factors for dark respiration ($^{18}\varepsilon_{dark\_respi}$: - 17 ± 2 ‰) and photosynthesis ($^{18}\varepsilon_{photosynthesis}$: + 6.7 ± 3.3 ‰) are consistent with literature values, though the relatively large uncertainties highlight some current limitations, including suboptimal performance of the optical spectrometry and excessive calibration time. Stability tests of the

calibration gases indicated that less frequent calibrations (e.g., measuring both gases twice daily and one calibration gas every 15 – 20 minutes) would be sufficient to ensure accuracy.

Our automated system has significant potential for broader applications. First, its open-code design and use of relatively low-cost sensors (excluding the optical spectrometry analyzer) make it easily adaptable to other biological experiments. Second, coupling this system with other optical spectrometers, such as Picarro or Los Gatos Research (LGR) trace gas instruments, could enable the quantification of trace gas exchanges, including N_2O and CH_4 (and their isotopologues), between the plant/soil system and the atmosphere.

Future studies should focus on upgrading the instrumentation to enhance performance and reduce uncertainties in isotopic fractionation measurements. Additionally, optimizing calibration frequency will improve experimental efficiency and reliability. This system paves the way for more comprehensive and systematic investigations into gas exchange processes under diverse conditions.

Author contributions

AL and CPi designed the project. CPi, JS, SD and CPa carried out experiments at ECOTRON of Montpellier and FP, CPa, RJ, AD and OJ at LSCE. CPa, CPi and AL analyzed the data from the optical spectrometer and CPa and AL analysed the data from IRMS. CPa, CPi and AL prepared the manuscript with contributions from AM.

Competing interests

The authors declare that they have no conflict of interest.

Acknowledgements

The research leading to these results has received funding from the European Research Council under the European Union H2020 Programme (H2020/20192024)/ERC grant agreement no. 817493 (ERC ICORDA) and ANR HUMI17. The authors acknowledge the scientific and technical support of PANOPLY (Plateforme ANalytique géOsciences Paris-sacLaY), Paris-Saclay University, France. Our thanks also to go to AQUA-OXY (CNRS IIT project). This study benefited from the CNRS resources allocated to the French ECOTRONS Research Infrastructure, from the Occitanie Region and FEDER investments as well as from the state allocation 'Investissement d'Avenir' AnaEE- France ANR-11-INBS-0001. We would also like to thank Abdelaziz Faez and Olivier Ravel from ECOTRON of Montpellier for their help and Emeritus Prof. Phil Ineson from University of York.

References

Angert, A., Luz, B., and Yakir, D.: Fractionation of oxygen isotopes by respiration and diffusion in soils and its implications for the isotopic composition of atmospheric O_2, Global Biogeochem. Cy., 15, 871-880, https://doi.org/10.1029/2000GB001371, 2001.

545 Bender, M., Sowers, T., Dickson, M-L., Orchardo, J., Grootes, P., Mayewski, P. A., and Meese, D. A.:
546 Climate correlations between Greenland and Antarctica during the past 100,000 years, Nature, 372,
547 663-666, https://doi.org/10.1038/372663a0, 1994.
548
549 Blunier, T., Barnett, B., Bender, M. L., and Hendricks, M. B.: Biological oxygen productivity during the
550 last 60,000 years from triple oxygen isotope measurements, Global Biogeochem. Cy., 16, 3-4,
551 https://doi.org/10.1029/2001GB001460, 2002.
552
553 Capron, E., Landais, A., Lemieux-Dudon, B., Schilt, A., Loulergue, L., Buiron, D., Chappellaz, J., Masson-
554 Delmotte, V., Dahl-Jensen, D., Johnsen, S., Leuenberger, M., Oerter, S., H.: Synchronising EDML and
555 NorthGRIP ice cores using δ18O of atmospheric oxygen (δ18Oatm) and CH4 measurements over MIS
556 5 (80-123 ka), Quat. Sci. Rev., 29, 235-246, https://doi.org/10.1016/j.quascirev.2009.07.014, 2010.
557
558 Eisenstadt, D., Barkan, E., Luz, B., and Kaplan, A.: Enrichment of oxygen heavy isotopes during
559 photosynthesis in phytoplankton, Photosynth. Res., 103, 97-103,
560 https://doi.org/10.1007/s11120-009-9518-z, 2010.
561
562 Extier, T., Landais, A., Bréant, C., Prié, F., Bazin, L., Dreyfus, G., Roche, D. M., and Leuenberger, M.: On
563 the use of $\delta^{18}O_{atm}$ for ice core dating, Quat. Sci. Rev., 185, 244-257,
564 https://doi.org/10.1016/j.quascirev.2018.02.008, 2018.
565
566 Guy, R. D., Fogel, M.L., and Berry, J. A.: Photosynthetic fractionation of the stable isotopes of oxygen
567 and carbon, Plant Physiol., 101, 37-47, https://doi.org/10.1104/pp.101.1.37, 1993.
568
569 Helman, Y., Barkan, E., Eisenstadt, D., Luz, B., and Kaplan, A.: Fractionation of the three stables
570 oxygen isotopes by oxygen-producing and oxygen-consuming reactions in photosynthetic

organisms, Plant Physiol., 138, 2292-2298, https://doi.org/10.1104/pp.105.063768, 2005.

Keeling, R.F., and Shertz, S.R.: seasonal and interannual variations in atmospheric oxygen and implications for the global carbon cycle, Nature, 358, 723-727, https://doi.org/10.1038/358723a0, 1992.

Landais, A., Dreyfus, G., Capron, E., Masson-Delmotte, V., Sanchez-Goñi, M. F., Desprat, S., Hoffmann, G., Jouzel, J., Leuenberger M., and Johnsen, S.: What drives the orbital and millennial variations of $d^{18}O_{atm}$?, Quat. Sci. Rev., 29, 235-246, https://doi.org/10.1016/j.quascirev.2009.07.005, 2010.

Luz, B., and Barkan, E.: Assessment of Oceanic Productivity with the Triple-Isotope Composition of Dissolved Oxygen, Science, 288, 2028-2031, https://doi.org/10.1126/science.288.5473.2028, 2000.

Luz, B., Barkan, E., Bender, M. L., Thiemens, M. H., and Boering, K. A.: Triple-isotope composition of atmospheric oxygen as a tracer of biosphere productivity, Nature, 400, 547-550, https://doi.org/10.1038/22987, 1999.

Malaizé, B., Paillard, D., Jouzel, J., and Raynaud, D.: The Dole effect over the Last two glacial-interglacial cycles, J. Geophys. Res., 104, 14199-14208, https://doi.org/10.1029/1999JD900116, 1999.

Milcu, A., Allan, E., Roscher, C., Jenkins, T., Meyer, S. T., Flynn, D., Bessler, H., Buscot, F., Engels, C., Gubsch, M., König, S., Lipowsky, A., Loranger, J., Renker, C., Scherber, C., Schmid, B., Thébault, E., Wubet, T., Weisser, W. W., Scheu, S., and Eisenhauer, N.: Functionally and phylogenetically diverse plant communities key to soil biota, Ecology, 94, 1878-1885, https://doi.org/10.1890/12-1936.1, 2013.

Paul, C., Piel, C., Sauze, J., Pasquier, N., Prié, F., Devidal, S., Jacob, R., Dapoigny, A., Jossoud, O., Milcu, A., and Landais, A.: Determination of respiration and photosynthesis fractionation factors for atmospheric dioxygen inferred from a vegetation-soil-atmosphere analog of the terrestrial biosphere in closed chambers, Biogeosciences, https://doi.org/10.5194/bg-2021-324, 2023.

Piel, C., Romanini, D., Farradèche, M., Chaillot, J., Paul, C., Bienville, N., Lauwers, T., Sauze, J., Jaulin, K., Prié, F., and Landais, A.: High precision δ18O measurements of atmospheric dioxygen using optical-feedback cavity-enhanced absorption spectroscopy (OF-CEAS), Atmos. Meas. Tech. Discuss. [preprint], https://doi.org/10.5194/amt-2024-14, in review, 2024.

Severinghaus, J. P., Beaudette, R., Headly, M. A., Taylor, K. and Brook, E. J.: Oxygen-18 of O_2 records the impact of abrupt climate change on the terrestrial biosphere, Science, 324, 1431-1434, https://doi.org/10.1126/science.1169473, 2009.

Stolper, D. A., Bender, M. L., Dreyfus G. B., Yan Y., and Higgins J. A.: A Pleistocene ice core record of atmospheric O_2 concentrations, Science, 353, 1427-1430, https://doi.org/10.1126/science.aaf5445, 2016.

Stolper, D. A., Fischer, W. W., and Bender, M. L.: Effects of temperature and carbon source on the isotopic fractionations associated with O_2 respiration for $^{17}O/^{16}O$ and $^{18}O/^{16}O$ ratios in *E. coli*, Geochim. Cosmochim. Ac., 240, 152-172, https://doi.org/10.1016/j.gca.2018.07.039, 2018.

Werle, P.: Accuracy and precision of laser spectrometers for trace gas sensing in the presence of optical fringes and atmospheric turbulence, Appl Phys B, 102, 313-329, https://doi.org/10.1007/s00340-010-4165-9, 2011.

625

626

627

628

629

630

631